Supporting Information

Rearrangement of π-Electron Network and Switching of Edge-Localized π State in Reduced Graphene Oxide

Department of Chemistry, Tokyo Institute of Technology,

2-12-1 Ookayama, Meguro-ku, Tokyo 152-8551, Japan

Shintaro Fujii and Toshiaki Enoki

Table of contents

SI-1) LDA-calculated band structures for the models (2i), (2ii), (3i), (3ii), (7i), and (7ii)

DFT calculations were performed in the same way as describe in the main text using the rectangular graphene supercell containing 72 carbon atoms. The calculated band structures for the models of (2i), (2ii), (3i), (3ii), (7i), and (7ii) are shown in Figs. S1(a)-(f), respectively. The ON states for the models of (2i), (3i), and (7ii) are characterized by quasi-flat band(s) crossing the Fermi level, while the OFF states for the models of (2ii), (3ii), and (7i) do not have such flat bands.

SI-2) Estimation of the energy barrier between the ON and OFF states [models (6i) and (6ii) in Figures 5 and 6]

DFT calculations were performed within the local density approximation using the Perdew-Zunger exchange correlation scheme, as implemented in the CASTEP code [S1]. A rectangular graphene supercell containing 72 carbon atoms was used. The electronic wave functions were expanded in a plane-wave basis set with a cutoff kinetic energy of 25 Ry. Brillouin-zone integration was performed using a uniform 2 × 2 × 1 Monkhorst-type k-point grid. Linear synchronous transit/quadratic synchronous transit (LST/QST) methods [S2] were used to estimate the energy barrier between the ON and OFF states [see (6i) and (6ii) in Figures 5]. The atomic configurations were taken from the optimized structures shown in Figure 5. The total energy difference between the two configurations is ~−0.1 eV ($E_{6i} - E_{6ii}$). The calculated energy barrier height between the ON [6(i)] and OFF [6(ii)] states is ~0.8 eV (~20 kcal/mol); this acts as a moderate reaction barrier between the two states at room temperature (Figure S2). A reaction path was not found for switching between (7i) and (7ii) (Figure S3) because of the significant

steric interactions among the four carbonyl groups during the transition, which leads to large energetic destabilization; therefore, the transition between (7i) and (7ii) seems unlikely.

SI-3) Proposed oxidized defect models

To assess a wide variety of structural models that are subject to reversible structural changes with on-off switching of the localized π state, we began by considering simple models, such as an impurity adsorbed on the pristine graphene. DFT geometrical optimization was performed using the same conditions described above. The energy barriers were estimated according to the method used in SI-2.

(i) Chemical species adsorbed on the pristine graphene plane

DFT-LDA relaxed structures of the simple models where an impurity, such as an hydroxyl group (–OH) and epoxide group (–O–), is adsorbed onto the pristine plane are shown in Figures S4a–b. Dynamic structural switching between the two states can be caused by diffusion of the impurity on the pristine graphene plane; however, this does not induce switching of the localized π state because sublattice symmetry is preserved before and after the diffusion. As described in the main text, localized π states originate from the broken symmetry of the graphene bipartite lattice and therefore switching of the localized π states can be interpreted as a result of switching of the sublattice symmetry during structural change.

(ii) Vacancy modified with hydroxyl, epoxide, and carbonyl groups

Beyond the simple adsorbed impurity models, we considered oxidized monovacancy models. In addition to the hydroxyl and epoxide groups, carbonyl (–C=O) groups can form through the attachment of oxygen to under-coordinated carbon atoms at the edges. While there are a wide variety of oxidized defect models modified with chemical functional groups, such as –OH, –O–, and =O (*e.g.*, see some of the possible structures in Figures S4c–g), only a change of the bonding configurations, *i.e.*, between a sp^2-hybridized oxygen atom in the carbonyl group and sp^3-hybridized oxygen atom in the ether group, can cause rearrangement of the π-electron network without considerable energetic destabilization due to breakage of chemical bonds (*e.g.*, see the configurational switch from S4(d) to S4(e) in Fig. S4, in which one –OH group is removed from a vacancy-edge by making a σ-radical at the edge and is sat on an inner on-plane carbon site.) One example of the change of a sp^2-hybridized carbonyl group and sp^3-hybridized ether group is the interconvertible change between S4(f) and S4(g), which involves the conversion of one carbonyl group into an ether group. The change in bonding pattern leads to rearrangement of π-electron network, but does not induce on-off switching of the edge localized state. This can be intuitively explained by the sublattice symmetry: $\Delta N = |N_A - N_B| = 0$ for both S4(f) and S4(g). More generally, during the change from a carbonyl to an ether group, a pair of A and B atoms (π-sites) is removed from the π-electron network (see the π-site model of S4(k) and S4(l)). Thus, the sublattice symmetry is essentially maintained during the change in the bonding pattern. The switch of the edge localized state (*i.e.*, change in the sublattice symmetry) can be realized through a concerted reaction, in which the two carbonyl type configurations are converted into two ether type configurations [see models (3), (6) and (7) in Figure 5]. During this process, three A (B) and one B (A) sites are removed from the π-electron network (see the π-site models in Figures 6 (c) and (d)).

The energy barrier from (3ii) (OFF state) to (3i) (ON state) in Figure 5 was estimated to be ~2.6 eV based on the LST/QST methods (Figure S5). The high energy barrier height acts as a substantial reaction barrier and prevents switching between the ON and OFF states. The energetic instability of (3i) (ON state) is derived from steric interactions among the three oxygen atoms in the monovacancy defect and the corresponding upright orientation of the vacancy-edge carbon atoms. A similar steric hindrance effect is also evident for (7i) (OFF state) in the di-vacancy models (Figure 5). In contrast, the steric hindrance effect is significantly less for the (6i) (ON state), in which the ether group compactly fits into the graphene plane. It is evident that the out-of-plane deformation of the carbonyl groups in (6i) is less than that of the carbonyl groups in (3i) and (7i) (Figure 5).

In conjunction with the concerted reaction (Figure 6), another reaction path is possible, in which an ether group forms a bond to another carbon atom at the periphery of the vacancy edges [Figure S6(a)]. The energy barrier height from (6i) (ON state) to S4(h) (OFF state) is estimated to be ~1.2 eV (Figure S7), which is due to the instability of the transition state; this barrier height is substantially larger than that between (6i) and (6ii) (0.8 eV) (Figure S2) and could prevent the transition.

Here, we will focus on the diffusion paths of the ether group at the vacancy edges. In addition to the reaction path from the OFF to the ON state (Figure 6), other paths, in which the ether group (epoxide group) diffuses into the bulk are possible [Figures S6(b)]. The energy barriers along the paths toward S4(i) and S4(j) were calculated to be 1.8 and 1.4 eV, respectively (Figures S8 and

9). In contrast to the concerted reaction with a barrier <1 eV, which involves two oxygen atoms (Figure S2), the diffusion of a single oxygen atom destabilizes the transition state (Figures S8 and 9) leading to a substantial reaction barrier and preventing the diffusion toward S4(i) and S4(j) [Figure S6(b)]. Therefore, ether groups have a tendency to be trapped around the vacancy edges.

Based on the LDA-DFT calculations for the oxidized mono- and divacancy models, we found a variety of metastable structures due to the steric interactions among the oxygen-containing functional groups in the vacancy defect. Interconvertible structural switching events without considerable energetic loss due to the formation of dangling σ bonds are realizable *via* a switch in the bonding configuration of an oxygen atom between sp^2-hybridized and sp^3-hybridized forms. The local sublattice symmetry is conserved before and after changes in the bonding pattern based on the effective π-site model. A change in the sublattice symmetry (*i.e.*, on–off switching of the defect-localized states) can be induced by a cooperative change in the bonding configurations of two oxygen atoms between sp^3-hybridized and sp^2-hybridized forms at the edges. Within the DFT calculations for the models considered here, the on-off switching of the defect-localized defects can be basically explained by the sublattice symmetry using the effective π-site models. The cooperative reaction essentially reduces the reaction barrier height between the two states, which enables the reaction to be manipulated (*i.e.*, on–off switching of the edge localized states) by AFM. Among the proposed on–off switching models [(3), (6), and (7) in Figure 5], a moderate activation barrier height of <1 eV was found only for (6), in which the ether group (*i.e.*, substitutional oxygen in the graphene plane) plays an important role. The ether group effectively eliminates the steric hindrance among the remaining carbonyl functional

groups, which reduces the barrier height between the ON and OFF states to <1 eV [(6i) and (6ii)] and energetically stabilizes the ON state [(6i)].

Figure captions

Figure S1. DFT-calculated band structures along the high symmetry points (Y-G-X) for the models of (a) (2i), (b) (2ii), (c) (3i), (d) (3ii), (e) (7i), and (f) (7ii). The band structure of pristine graphene is represented by thin black lines and is superimposed on (a)-(f). The presence and absence of the quasi-flat bands near E_f (*i.e.*, edge-localized non-bonding states) are denoted by "ON" an "OFF" on the right corner in (a)-(f).

Figure S2. Reaction energy profile for switching between (6i) and (6ii) (Figure 5). Structural models are shown inset. Black and red balls represent carbon and oxygen atoms, respectively.

Figure S3. Top-down perspective of the structural models of (7i) and (7ii) (see Figure. 5 for (7i) and (7ii)).

Figure S4. a)-j) DFT-LDA relaxed structures for oxidized defect models. Black, red, and blue balls represent carbon, oxygen, and hydrogen atoms, respectively. k) and l) Effective π-site model of (f) and (g), respectively. Black and white balls represent the A(B) and B(A) graphene-sublattices, respectively.

Figure S5. Reaction energy profile for switching between (3i) and (3ii) (see Figure. 5 for (3i) and (3ii)). Structural models are shown inset.

Figure S6. a) Reaction path between (6i) (Figure 5) and S4(h) (Figure S4). Two carbonyl bonds at the vacancy edges of (6i) can be converted into two ether moieties to form S4(h) in a concerted manner. Electron movements are indicated by single-headed arrows. b) Diffusion paths of the ether group (epoxide group) in (6ii) (Figure 5). Two possible paths are indicated by arrows. Oxygen diffusion along path_1 and path_2 lead to the formation of S4(i) and S4(h), respectively.

Figure S7. Reaction energy profile for switching between (6i) (Figure 5) and S4(h) (Figure S4).

Figure S8. Reaction energy profile for switching between (6ii) (Figure 5) and S4(i) (Figure S4).

Figure S9. Reaction energy profile for switching between (6ii) (Figure 5) and S4(j) (Figure S4).

References

[S1] Clark, S. J.; Segall, M. D.; Pickard, C. J.; Hasnip, P. J.; Probert, M. I. J.; Refson, K.; Payne, M. C. First Principles Methods Using CASTEP. *Z. Kristallogr*. **2005**, *220*, 567-570.

[S2] Govind N.; Petersen, M.; Fitzgerald, G.; Smith, D. K.; Andzelm, J. A Generalized Synchronous Transit Method for Transition State Location. *Comp. Mater. Sci*. **2003**, *28*, 250-258.

Figure S1

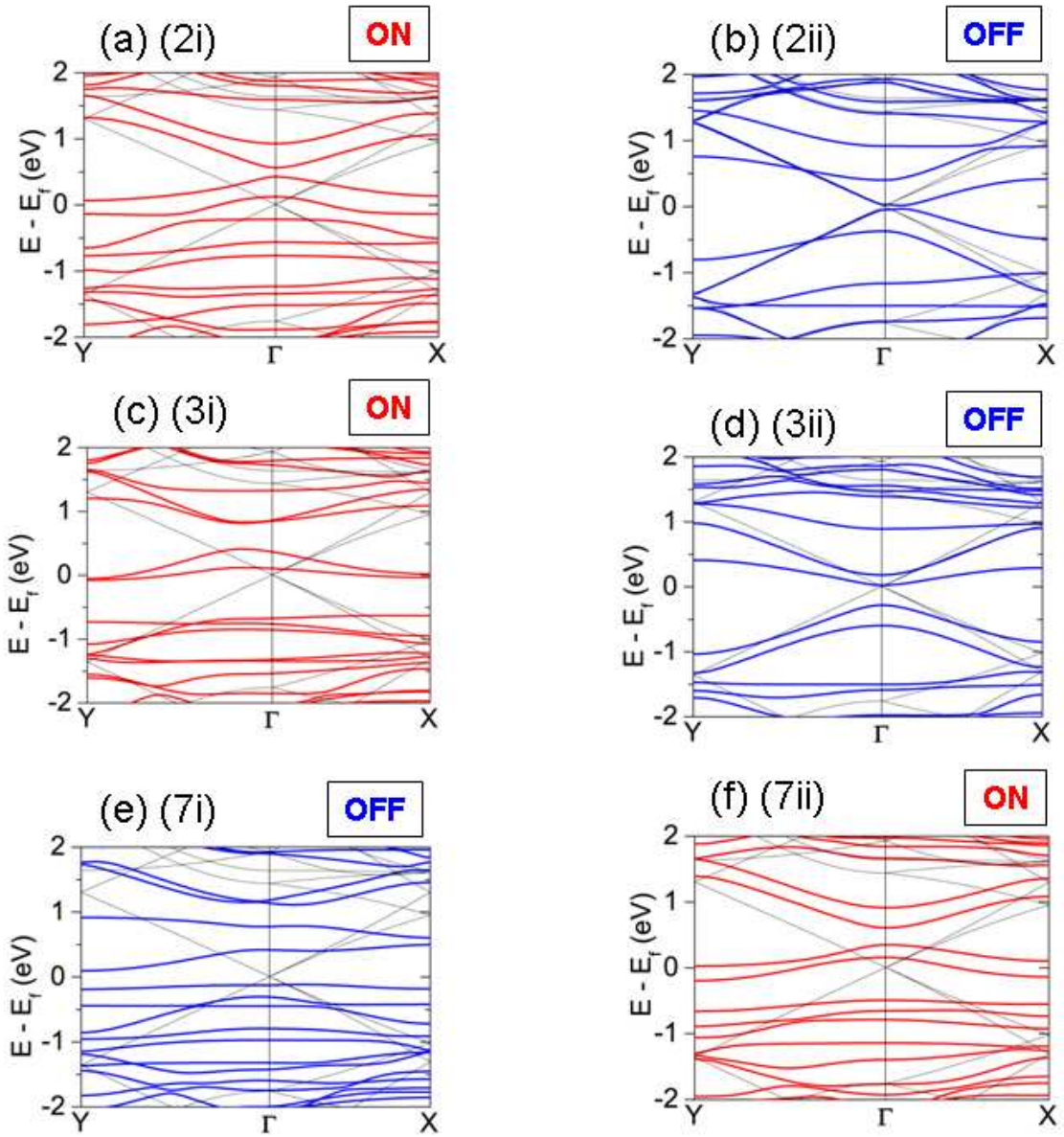

Figure S2

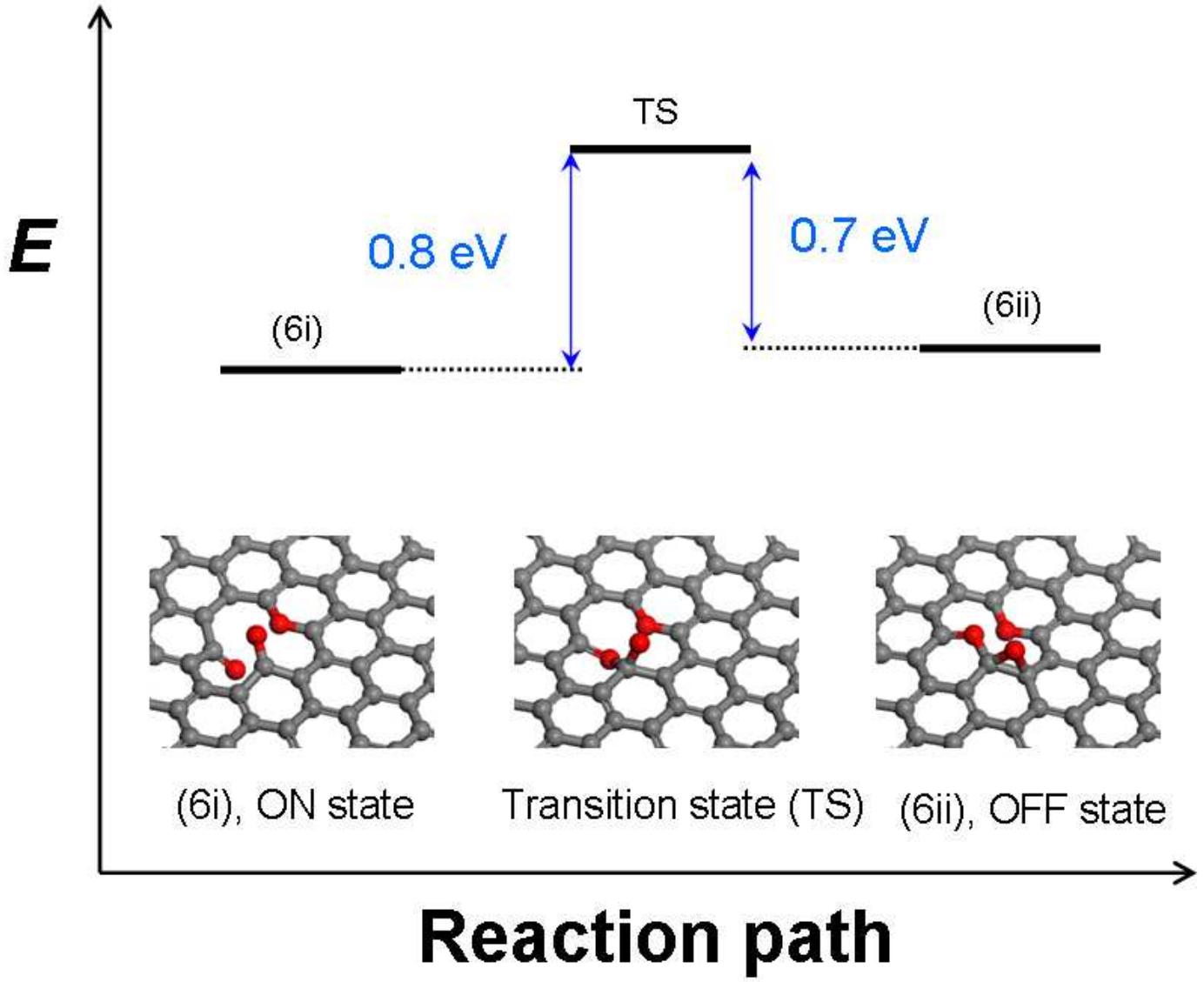
E
TS
0.8 eV
0.7 eV
(6i)
(6ii)
(6i), ON state
Transition state (TS)
(6ii), OFF state
Reaction path

Figure S3

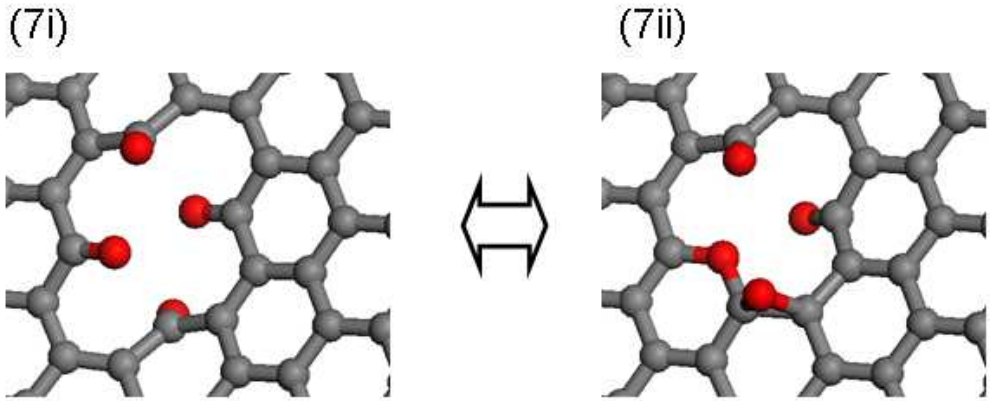

Figure S4

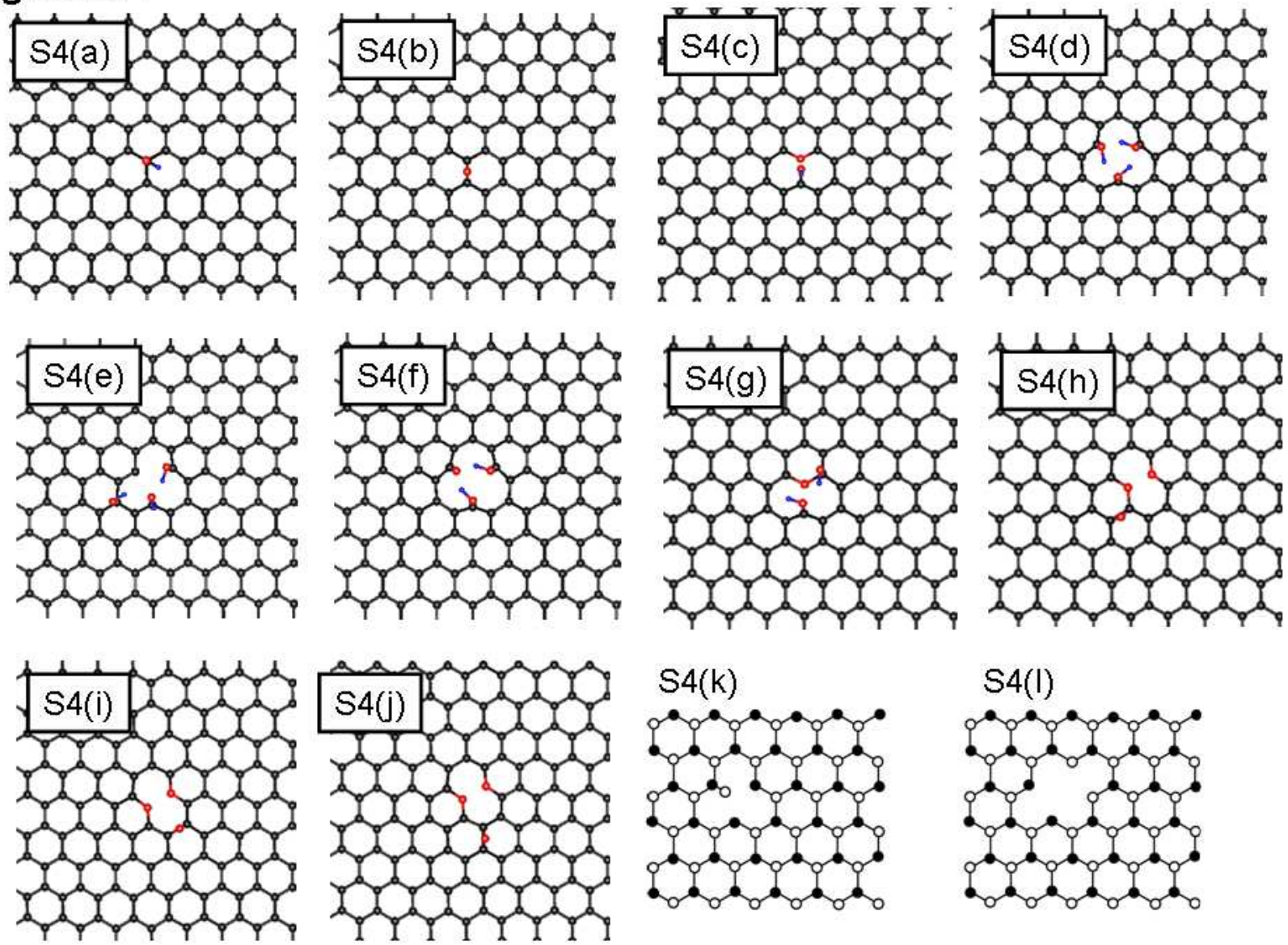

Figure S5

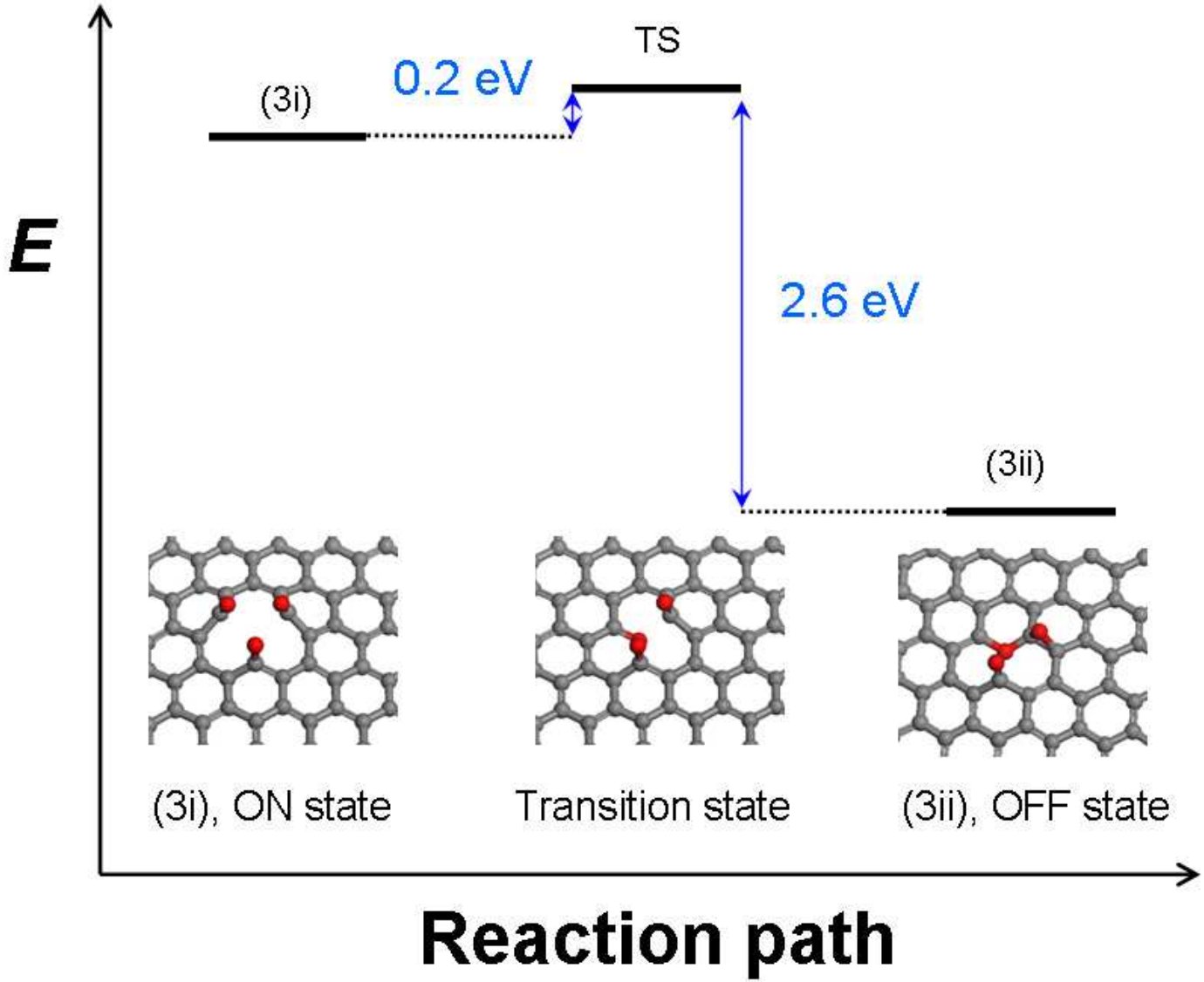
TS
0.2 eV
(3i)
E
2.6 eV
(3ii)
(3i), ON state
Transition state
(3ii), OFF state
Reaction path

Figure S6

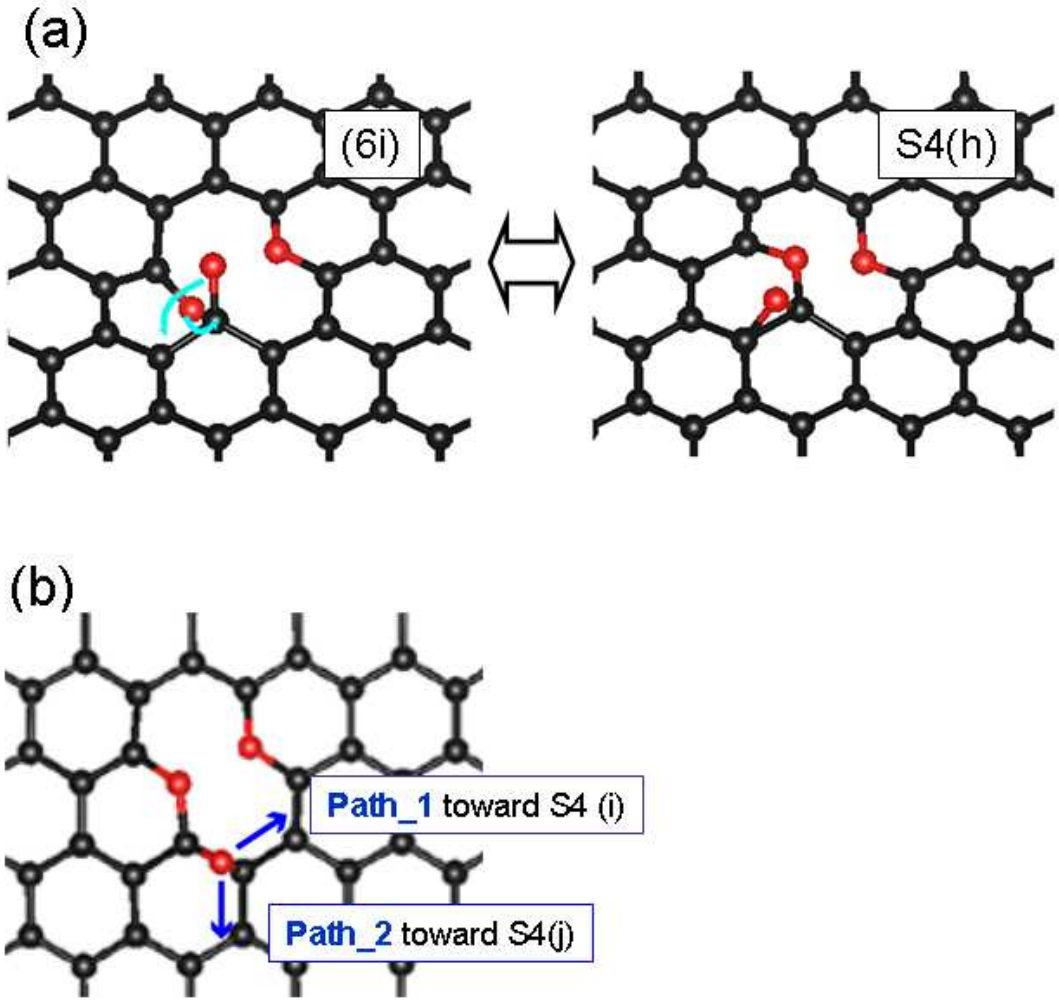

Figure S7

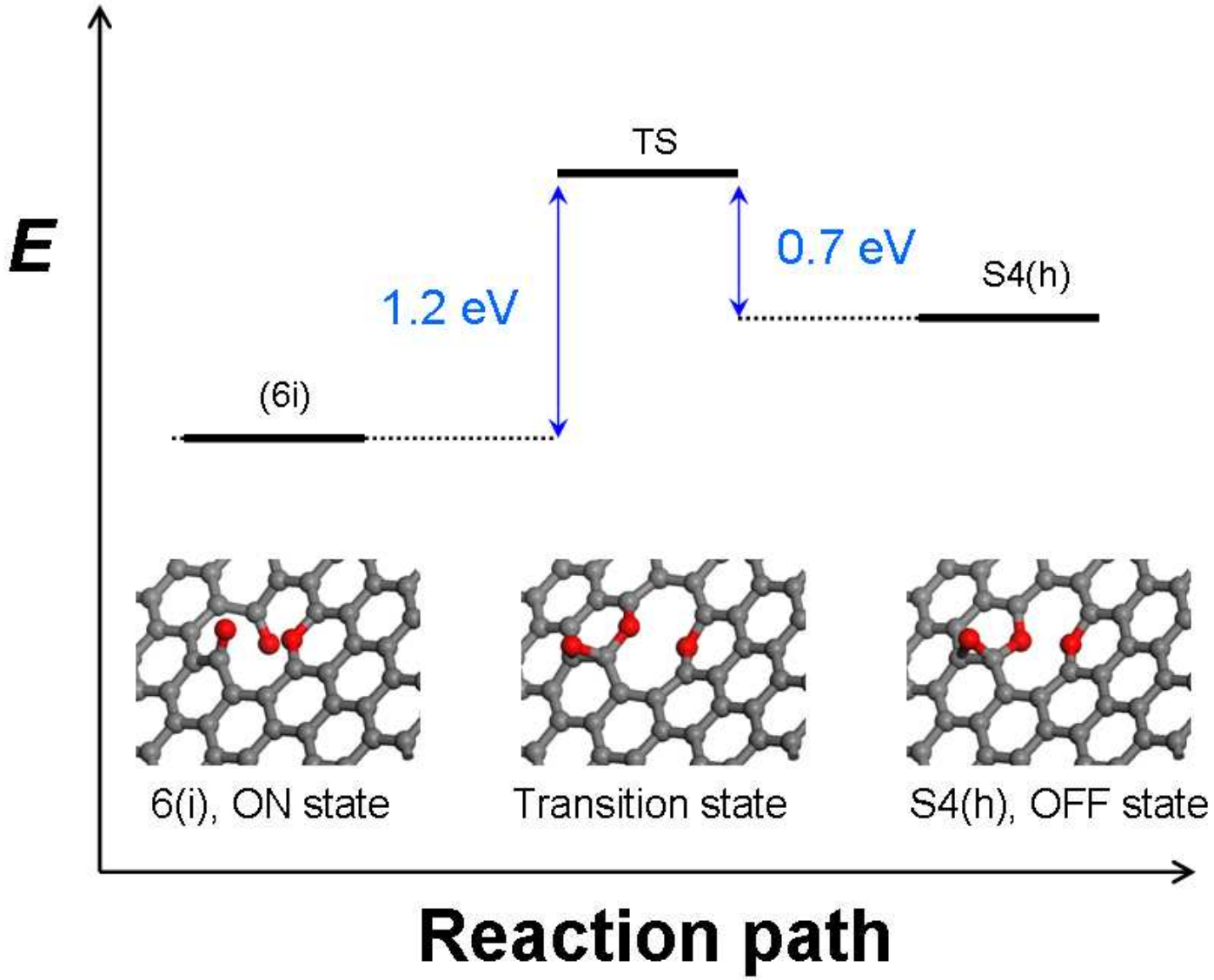
E
TS
0.7 eV
S4(h)
1.2 eV
(6i)
6(i), ON state
Transition state
S4(h), OFF state
Reaction path

Figure S8

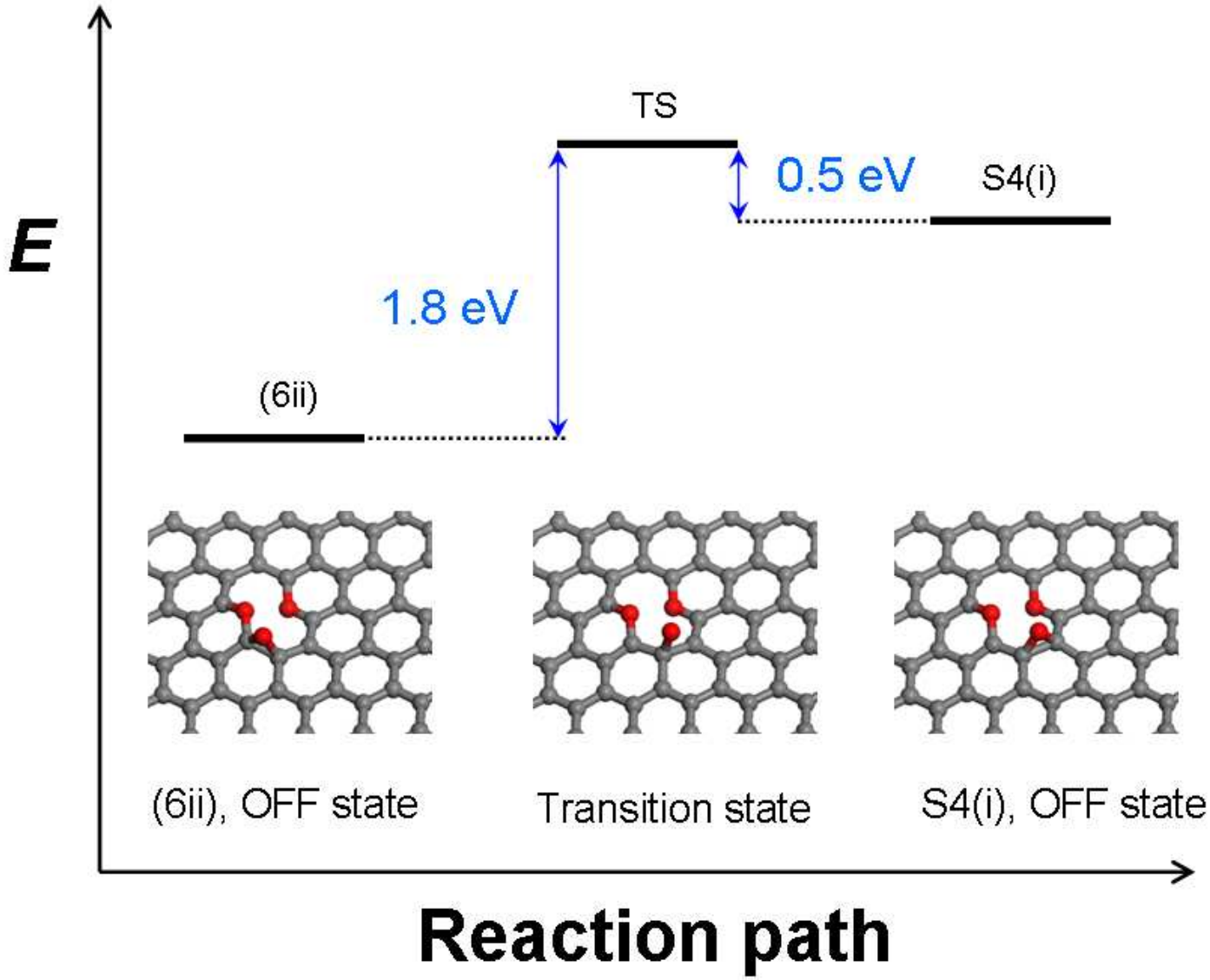
E
TS
0.5 eV
S4(i)
1.8 eV
(6ii)
(6ii), OFF state
Transition state
S4(i), OFF state
Reaction path

Figure S9

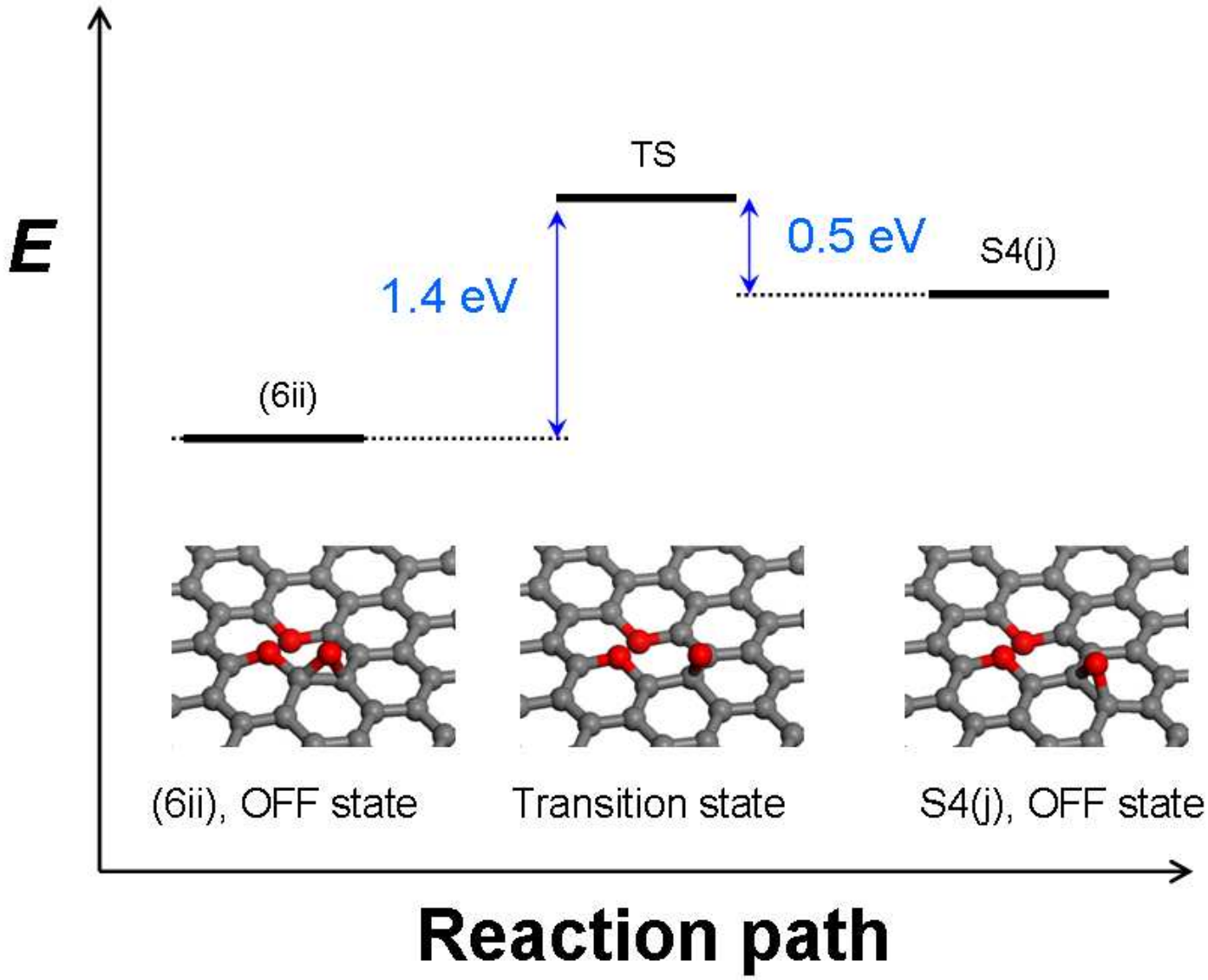
E
TS
0.5 eV
S4(j)
1.4 eV
(6ii)
(6ii), OFF state
Transition state
S4(j), OFF state
Reaction path